Supporting Information

Mechanistic Understanding of the Antimony-Bismuth Alloy Promoted Electrocatalytic CO_2 Reduction to Formate

Jiameng Sun,[a] Wanfeng Yang,[b] Bin Yu,[a] Yalong Liu,[a] Yong Zhao,[c,*] Guanhua Cheng,[a] Zhonghua Zhang,[a,*]

[a]Key Laboratory for Liquid-Solid Structural Evolution and Processing of Materials (Ministry of Education), School of Materials Science and Engineering, Shandong University, Jingshi Road 17923, Jinan 250061, P.R. China

[b]Department of Chemistry, City University of Hong Kong, Hong Kong SAR, P.R. China

[c]CSIRO Energy Centre, 10 Murray Dwyer Circuit, Mayfield West NSW2304, Australia

*Corresponding authors. Email: zh_zhang@sdu.edu.cn (Z.H. Zhang); Y.Zhao@csiro.au (Y. Zhao)

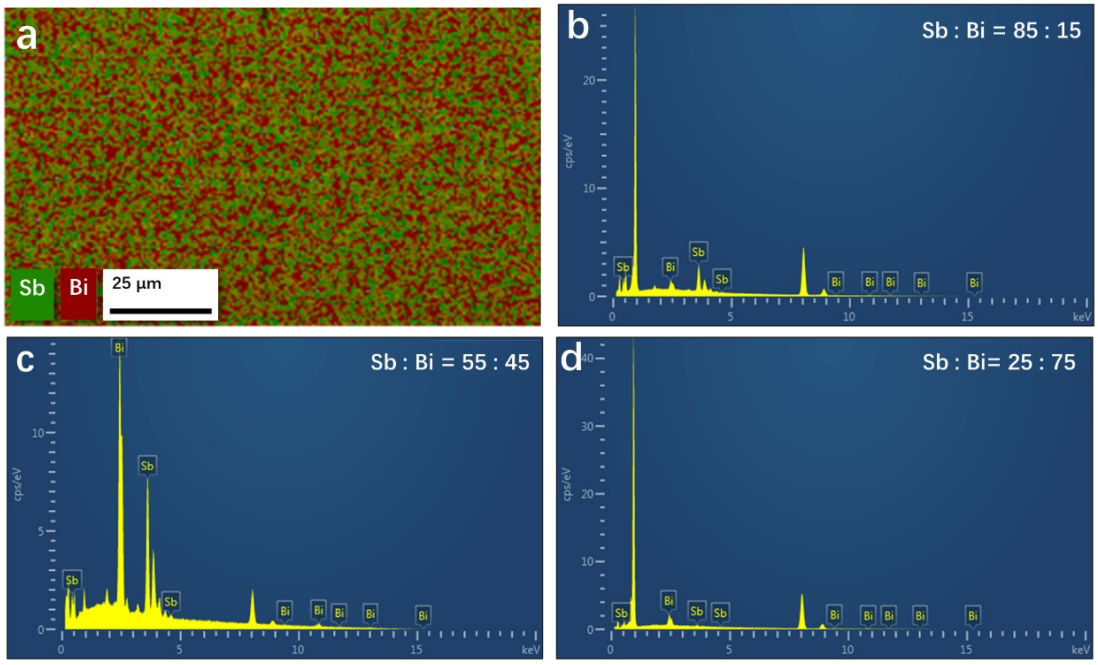

Figure S1. (a) EDX mapping image of the $Sb_{55}Bi_{45}$ catalyst. (b-d) Typical EDX spectra of Sb-Bi films with different element concentrations.

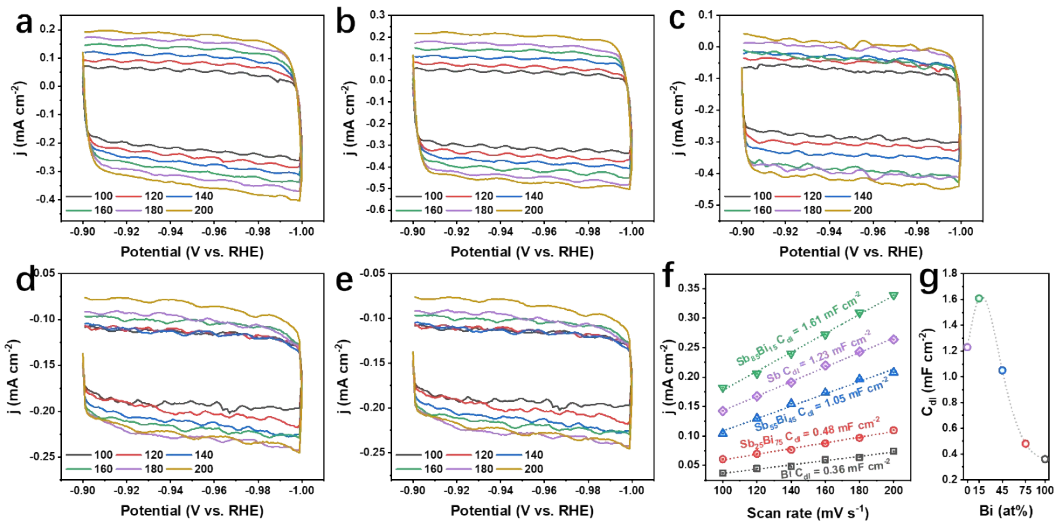

Figure S2. Electrochemical capacitance measurements to determine the ECSAs of electrodes. Cyclic voltammetry (CV) measured at different scan rates of (a) Sb, (b) $Sb_{85}Bi_{15}$, (c) $Sb_{55}Bi_{45}$, (d) $Sb_{25}Bi_{75}$ and (e) Bi catalysts. (f) Measured capacitive current densities based on the CV curves in (a-e) plotted as a function of scan rates. (g) Measured capacitive current densities based on the cyclic voltammetry (CV) curves in (f) plotted as a function of Bi content.

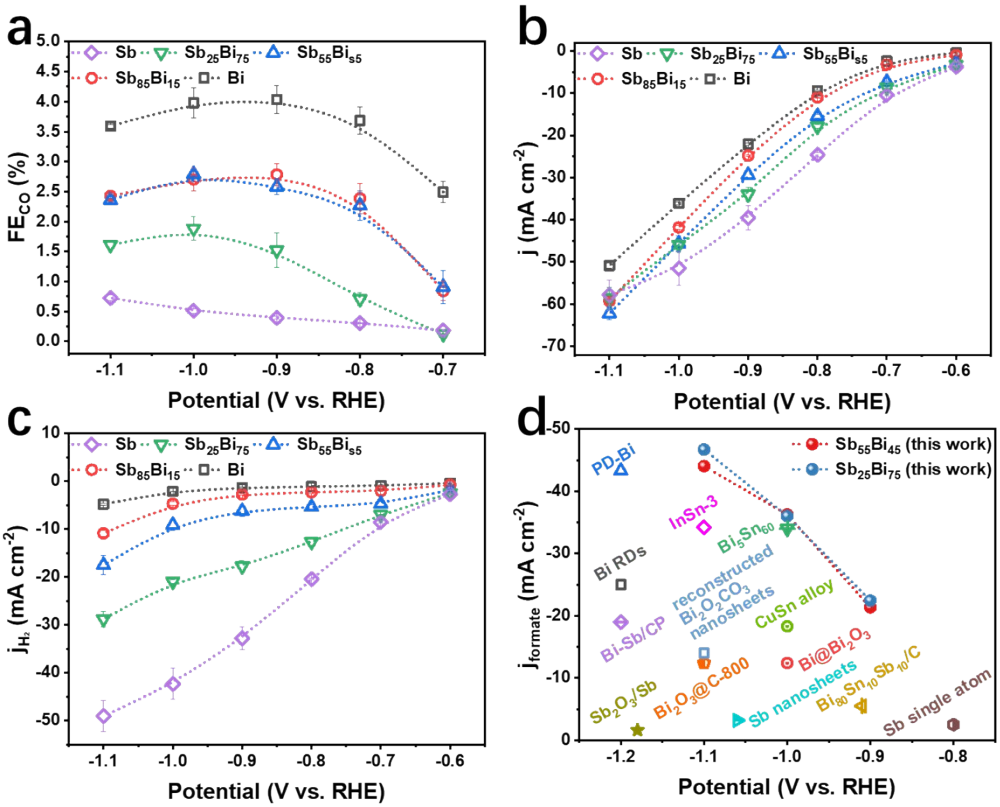

Figure S3. (a) FE of CO, (b) j, (c) j of H_2 plots for the pure Bi, Sb and Sb-Bi alloy catalysts in 0.5 M $KHCO_3$. (d) Comparison of various Bi,Sb-based and other formate-formation electrocatalysts for CO_2R to formate conducted in the H-type cell.

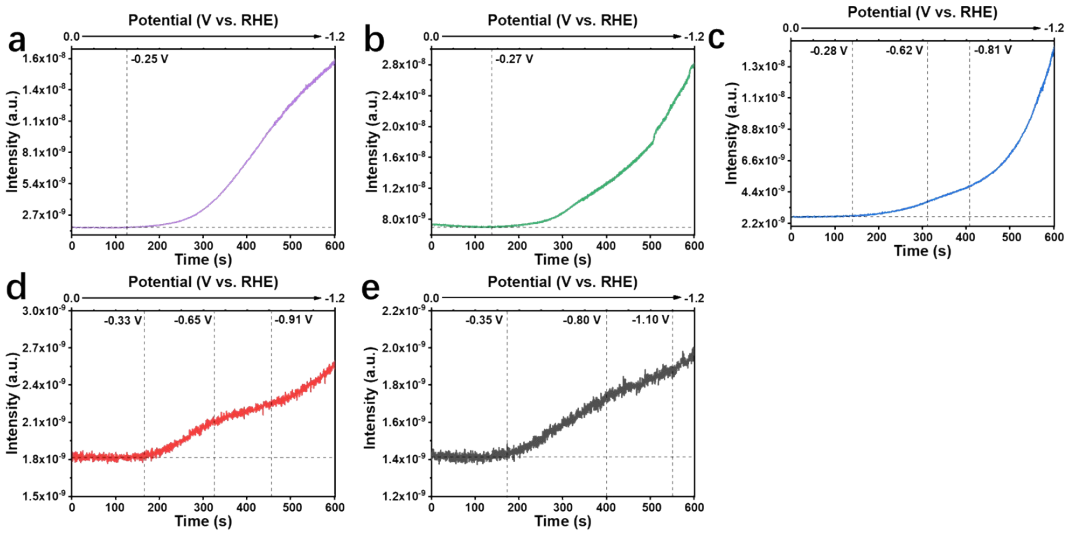

Figure S4. The on-line DEMS results over (a) Sb, (b) $Sb_{85}Bi_{15}$, (c) $Sb_{55}Bi_{45}$, (d) $Sb_{25}Bi_{75}$ and (e) Bi catalysts for H_2 (m/z = 2) under LSV measurements from 0 to –1.1 V vs. RHE at a scan rate of 2 mV s^{-1} in 1 M KOH.

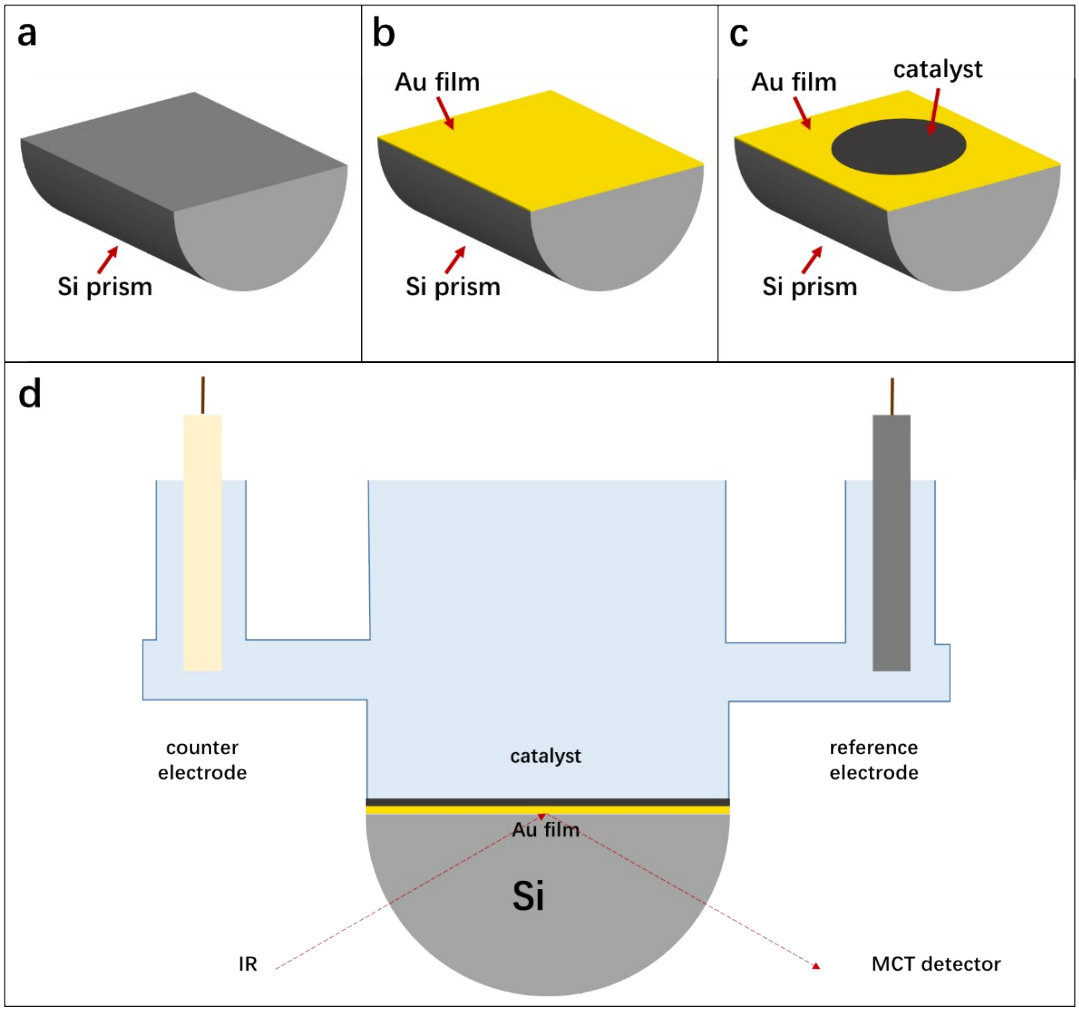

Figure S5. Schematic illustrations of (a) Si prism, (b) Si prism with Au film for surface enhancement and (c) sputtered alloy catalyst on the Si prism with Au film. (d) Diagram of in-situ ATR-SEIRAS measurements.

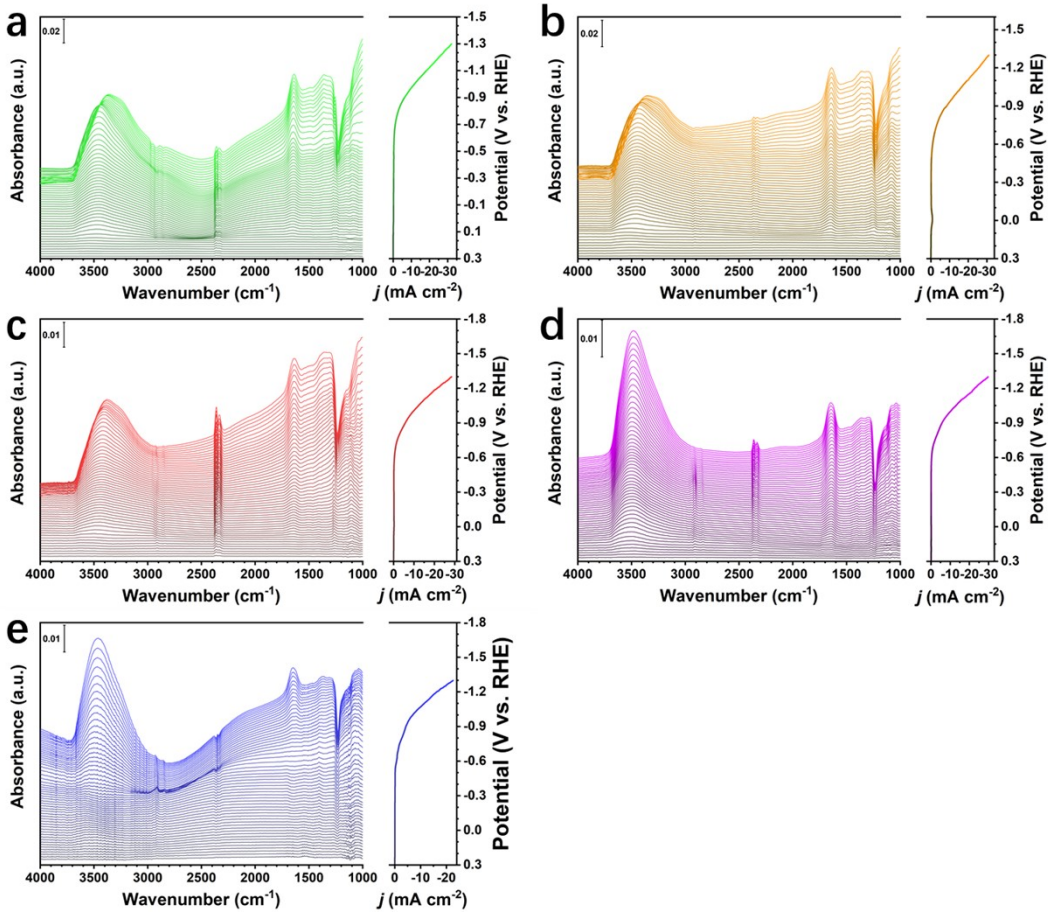

Figure S6. Complete in-situ ATR-SEIRAS spectra on the surface of (a) Sb, (b) $Sb_{85}Bi_{15}$, (c) $Sb_{55}Bi_{45}$, (d) $Sb_{25}Bi_{75}$ and (e) Bi catalysts during LSV measurements in CO_2-saturated 0.5 M $KHCO_3$ electrolyte from 0.3 to –1.3 V vs. RHE.

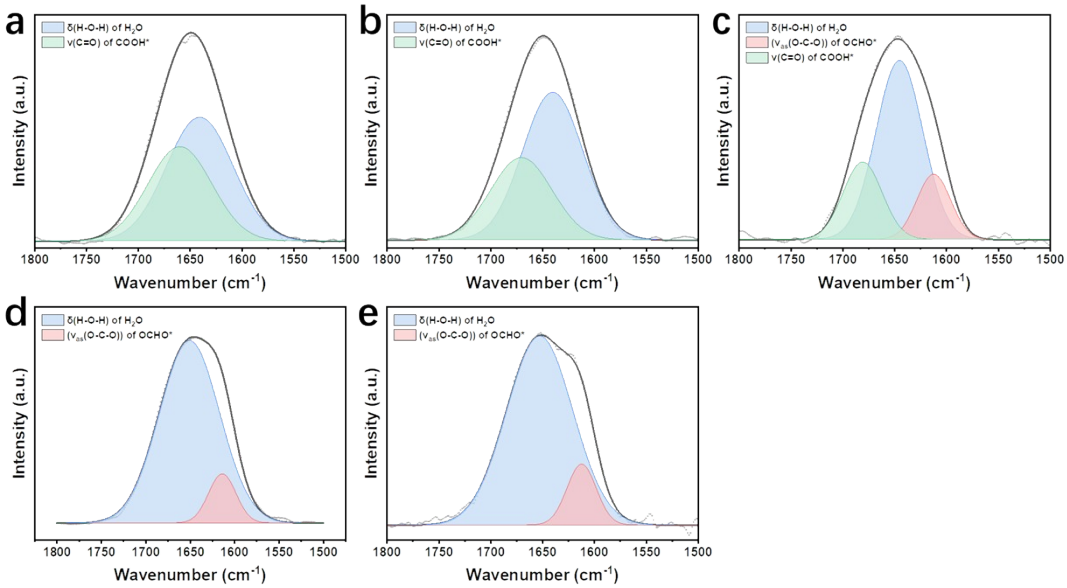

Figure S7. Partial in-situ ATR-SEIRAS spectra and the fitting results on the surface of (a) Sb, (b) $Sb_{85}Bi_{15}$, (c) $Sb_{55}Bi_{45}$, (d) $Sb_{25}Bi_{75}$ and (e) Bi catalysts from Figure S6.

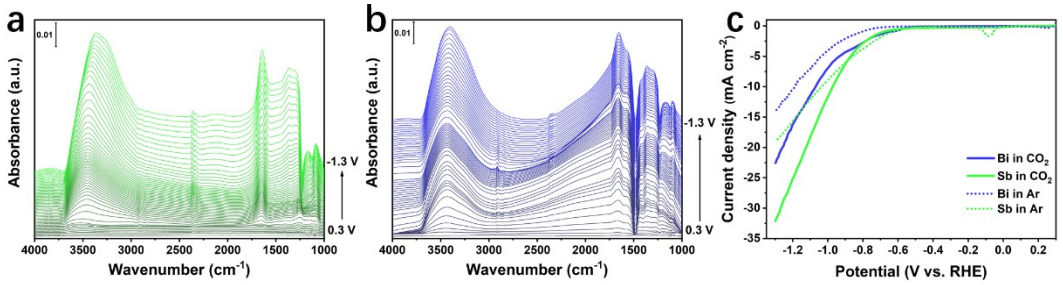

Figure S8. Complete in-situ ATR-SEIRAS spectra on the surface of (a) Sb and (b) Bi catalysts during LSV measurements in Ar-saturated 0.5 M $KHCO_3$ electrolyte from 0.3 to –1.3 V vs. RHE. (c) LSV pots in CO_2 and Ar environment for pure Sb and Bi catalysts.

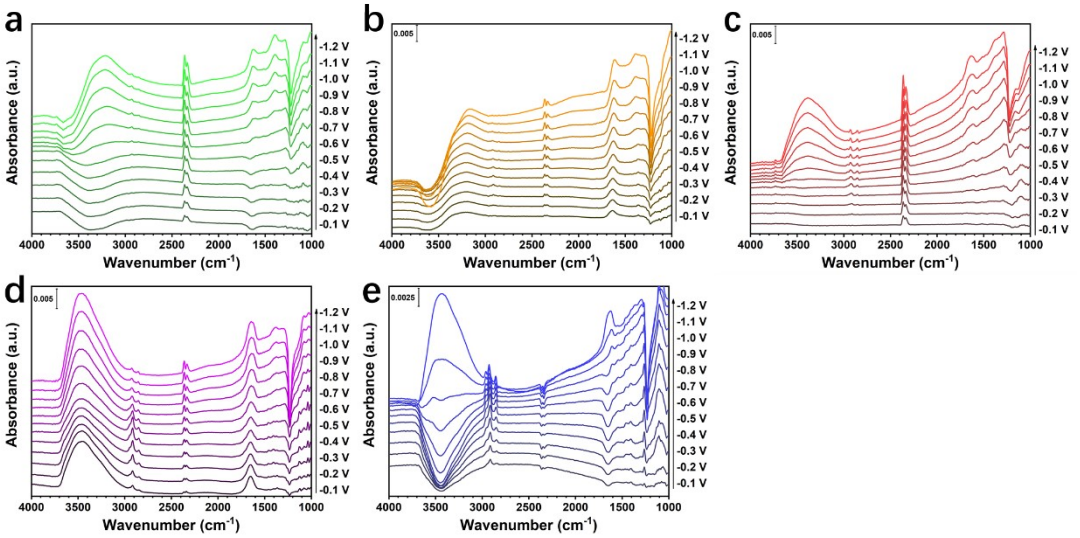

Figure S9. In-situ ATR-SEIRAS spectra on the surface of (a) Sb, (b) $Sb_{85}Bi_{15}$, (c) $Sb_{55}Bi_{45}$, (d) $Sb_{25}Bi_{75}$ and (e) Bi catalysts under different applied potentials.

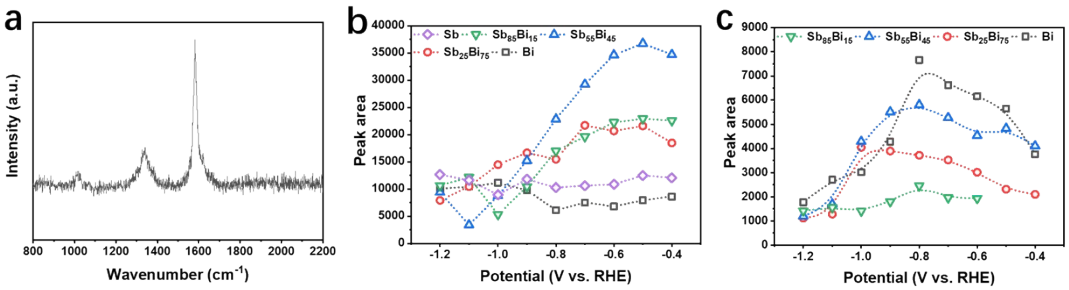

Figure S10. (a) Raman spectra of CFP in CO_2-saturated $KHCO_3$. The peak area of adsorption (b) HCO_3^- and (c) CO_3^{2-} band for Sb, Bi and Sb-Bi alloy catalysts.

Table S1. Comparison of various Bi,Sb-based and other formate-formation electrocatalysts for CO_2RR to formate conducted in the H-type cell.

Catalysts	Electrolyte	Potential (V vs. RHE)	*j* of formate (mA cm^{-2})	References
$Sb_{55}Bi_{45}$	**0.5 M $KHCO_3$**	**-1.0**	**-36.3**	**this work**
		-1.1	**-45.1**	**this work**
$Sb_{75}Bi_{25}$	**0.5 M $KHCO_3$**	**-1.0**	**-36.0**	**this work**
		-1.1	**-46.7**	**this work**
Bi	0.5 M $KHCO_3$	-1.0	-32.6	this work
Sb	0.5 M $KHCO_3$	-1.0	-9.0	this work
Bi RDs	0.5 M $KHCO_3$	-1.2	-25.0	[1]
Bi_2O_3@C-800	0.5 M $KHCO_3$	-1.1	-12.4	[2]
Bi@Bi_2O_3	0.5 M $KHCO_3$	-1.0	-22.9	[3]
PD-Bi	0.5 M $KHCO_3$	-1.2	-43.3	[4]
Bi_5Sn_{60}	0.1 M $KHCO_3$	-1.0	-34.0	[5]
$Bi_{80}Sn_{10}Sb_{10}$/C	0.45 M $KHCO_3$ and 0.5 M KCl	-0.91	-5.5	[6]
Bi-Sb/CP	0.5 M $KHCO_3$	-1.2	~-19	[7]
reconstructed $Bi_2O_2CO_3$ nanosheets	0.5 M $KHCO_3$	-1.1	~-14	[8]
Sb nanosheets	0.5 M $NaHCO_3$	-1.06	-3.2	[9]
Sb single atom	0.5 M $KHCO_3$	-0.8	-2.5	[10]
Sb_2O_3/Sb	0.5 M KCl	-1.18	-1.6	[11]
CuSn alloy	0.5 M $KHCO_3$	-1.0	-18.3	[12]
InSn-3	0.5 M $KHCO_3$	-1.1	-34.2	[13]

References:

1. H. Xie, T. Zhang, R. Xie, Z. Hou, X. Ji, Y. Pang, S. Chen, M.M. Titirici, H. Weng, G. Chai, *Advanced Materials*, 2021, **33**, e2008373.

2. P. Deng, F. Yang, Z. Wang, S. Chen, Y. Zhou, S. Zaman, B.Y. Xia, *Angewandte Chemie International Edition*, 2020, **59**, 10807-10813.

3. P. Deng, H. Wang, R. Qi, J. Zhu, S. Chen, F. Yang, L. Zhou, K. Qi, H. Liu, B.Y. Xia, *ACS Catalysis*, 2019, **10**, 743-750.

4. Y. Xing, H. Chen, Y. Liu, Y. Sheng, J. Zeng, Z. Geng, J. Bao, *Chemical Communications*, 2021, **57**, 1502-1505.

5. Z. Li, Y. Feng, Y. Li, X. Chen, N. Li, W. He, J. Liu, *Chemical Engineering Journal*, 2022, **428**, 130901.

6. B. Ávila-Bolívar, V. Montiel, J. Solla-Gullón, *ChemElectroChem*, 2022, **9**, e202200272.

7. C. Yang, Y.R. Hu, S.X. Li, Q. Huang, J. Peng, *ACS Applied Materials & Interfaces*, 2023, **15**, 6942-6950.

8. S.L. Zhao, Y. Qin, X.R. Wang, C. Wang, X. Chen, Y. Wang, J.X. Yu, X.J. Liu, Y.P. Wu, Y.H. Chen, *Small*, 2023, **19**, 2302878.

9. F. Li, M. Xue, J. Li, X. Ma, L. Chen, X. Zhang, D.R. MacFarlane, J. Zhang, *Angewandte Chemie International Edition*, 2017, **129**, 14910-14914.

10. Z. Jiang, T. Wang, J. Pei, H. Shang, D. Zhou, H. Li, J. Dong, Y. Wang, R. Cao, Z. Zhuang, *Energy & Environmental Science*, 2020, **13**, 2856-2863.

11. B. Ávila-Bolívar, V. Montiel, J. Solla-Gullón, *Journal of Electroanalytical Chemistry*, 2021, **895**, 130901.

12. B.X. Ning, W.J. Chang, M.M. Liu, H. Jiang, C.Z. Li, *ChemElectroChem*, 2021, **8**, 1150-1155.

13. J.G. Wang, S.L. Ning, M. Luo, D. Xiang, W. Chen, X.W. Kang, Z. Jiang, S.W. Chen, *Applied Catalysis B-Environmental*, 2021, **288**, 119979.